

Extreme tsunami inundation in Hawai‘i from Aleutian–Alaska subduction zone earthquakes

Rhett Butler¹  · David Walsh² · Kevin Richards³

Received: 27 September 2016 / Accepted: 27 October 2016 / Published online: 17 November 2016
© The Author(s) 2016. This article is published with open access at Springerlink.com

Abstract The 2011 Tohoku earthquake and tsunami motivated an analysis of the potential for great tsunamis in Hawai‘i that significantly exceed the historical record. The largest potential tsunamis that may impact the state from distant, Mw 9 earthquakes—as forecast by two independent tsunami models—originate in the Eastern Aleutian Islands. This analysis is the basis for creating an extreme tsunami evacuation zone, updating prior zones based only on historical tsunami inundation. We first validate the methodology by corroborating that the largest historical tsunami in 1946 is consistent with the seismologically determined earthquake source and observed historical tsunami amplitudes in Hawai‘i. Using prior source characteristics of Mw 9 earthquakes (fault area, slip, and distribution), we analyze parametrically the range of Aleutian–Alaska earthquake sources that produce the most extreme tsunami events in Hawai‘i. Key findings include: (1) An Mw 8.6 ± 0.1 1946 Aleutian earthquake source fits Hawai‘i tsunami run-up/inundation observations, (2) for the 40 scenarios considered here, maximal tsunami inundations everywhere in the Hawaiian Islands cannot be generated by a single large earthquake, (3) depending on location, the largest inundations may occur for either earthquakes with the largest slip at the trench, or those with broad faulting over an extended area, (4) these extremes are shown to correlate with the frequency content (wavelength) of the tsunami, (5) highly variable slip along the fault strike has only a minor influence on inundation at these tele-tsunami distances, and (6) for a given maximum average fault slip, increasing the fault area does not generally produce greater run-up, as the additional wave energy enhances longer wavelengths, with a modest effect on inundation.

✉ Rhett Butler
rgb@hawaii.edu

¹ Hawai‘i Institute of Geophysics and Planetology, University of Hawai‘i at Mānoa, 1680 East-West Road, POST 602, Honolulu, HI, USA

² Pacific Tsunami Warning Center, NOAA Inouye Regional Center, 1845 Wasp Boulevard, Building 176, Honolulu, HI 96816, USA

³ Hawaii Emergency Management Agency, 3949 Diamond Head Road, Honolulu, HI 96816-4495, USA

Keywords Tsunami modeling · 1946 tsunami · Earthquake source mechanisms · Tsunami inundation · North Pacific, Aleutian Islands, and Hawai‘i

1 Introduction

The March 11, 2011, great Tohoku earthquake and tsunami in Japan served as a wake-up call to coastal communities in the Pacific, re-emphasizing the lesson learned in the Indian Ocean in 2004: the potential for a giant Mw 9 earthquake to inflict a devastating tsunami both locally and across the ocean. The State of Hawaii was largely spared great damage (\$30.6M, National Centers for Environmental Information 2016) from the Tohoku tsunami, and statewide evacuation zones were sufficient. However, as TV showed in real time, the tsunami waves approaching the Japanese coast, overtopping the carefully planned and constructed system of seawalls, inundating cities and the countryside, and severely damaging a nuclear power plant, the question posed by Butler (2012) is whether Hawai‘i is prepared for a worst-case scenario like Tohoku.

Located in the middle of the Pacific, Hawai‘i is susceptible to tsunamis from all directions along the “ring of fire” of the Pacific, bounded by subduction zones with the potential for giant earthquakes. Damaging tsunamis, often lethal, have impacted Hawai‘i from Japan, Kamchatka, the Aleutian Islands, Alaska, and Chile (Fig. 1). Although these events include 4 of the 5 largest earthquakes ($M_w \geq 9$) since the invention of the Richter scale—the 5th occurred in the Indian Ocean—the largest earthquakes have not produced Hawai‘i’s largest tsunamis. This distinction belongs to the two Mw 8.6 events in the Aleutian Islands (Fig. 2). Furthermore, a review of prior Aleutian earthquakes (Butler

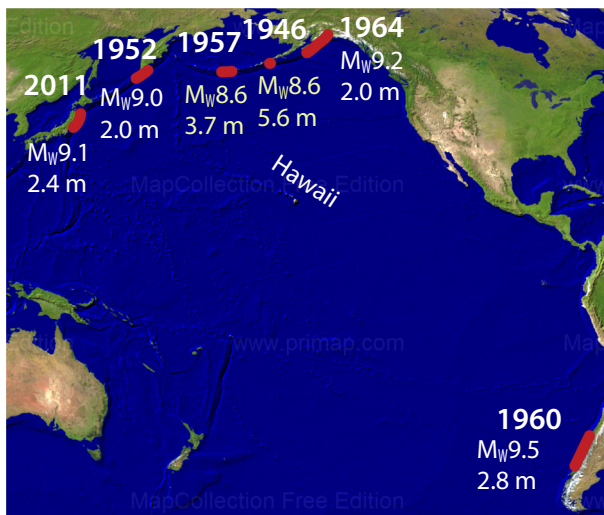


Fig. 1 Historic earthquakes resulting in destructive tsunamis in Hawai‘i are shown. Approximate fault areas are noted in red, with year of occurrence, magnitude (M_w), and average run-up in Hawai‘i. *NB* the largest tsunamis were not from the giant $M_w \geq 9$ earthquakes, but rather from two Mw 8.6 Aleutian earthquakes

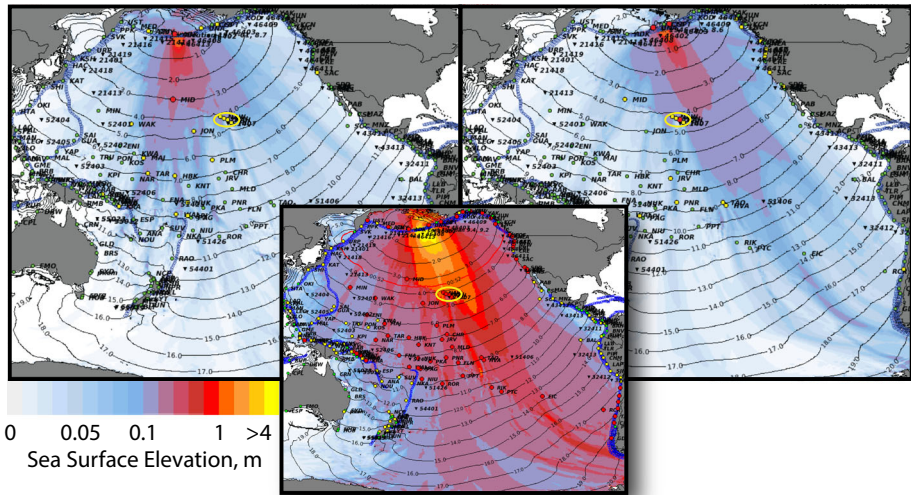


Fig. 2 Three tsunami forecasts of maximum sea-surface elevation (m) are shown: (left) the 1957 tsunami from the Mw 8.6 earthquake; (right) the 1946 tsunami from the Mw 8.6 earthquake; and (center) a hypothetical Mw 9.25 earthquake and tsunami originating in the Eastern Aleutians between the 1957 and 1946 sources. *Yellow ellipses encircle* the Hawaiian Islands, which lie directly in the path of an Eastern Aleutian event. Although the 1946 and 1957 tsunamis were the two largest historical tsunamis in Hawai‘i, they were directed east and west of the islands, respectively

2012) shows that the Eastern Aleutians region is capable of a giant Mw 9+ earthquake along a section of the Aleutian island arc directly facing Hawai‘i.

The bases for the danger to Hawai‘i from the Aleutians are threefold: tectonics, proximity, and geometry. The Aleutian subduction zone is very seismogenically active, with three Mw ≥ 8.6 earthquakes since 1946. The tsunami propagation time from there to Hawai‘i is a short, 4.5 h—imparting the minimum warning time for all non-local tele-tsunamis. Finally, the arcuate Aleutians are geometrically situated to focus tsunami energy toward Hawai‘i (e.g., Titov et al. 1999, 2001; Tang et al. 2006). These points are illustrated in Fig. 2, where the observed tsunami energy from the 1946 and 1957 events skirted the Hawaiian Islands, propagating to the east and west of the Islands, respectively. Between these two epicenters lies the possibility for an extreme Mw ~9 event (Butler 2012) that would be far more devastating than either the 1946 or 1957 tsunamis.

In order to meet this threat, the Hawaii State Civil Defense (now Emergency Management Agency) engaged with the lead author (R.B.) to work with the Pacific Tsunami Warning Center and the Hawai‘i Mapping Project to formulate the maximum credible tsunamigenic earthquake(s) threatening the Hawai‘i coast. After “appropriate and prudent” review by the U.S. Geological Survey looking at Hawaii’s risk, these extreme earthquakes were to be used as the basis for updated tsunami evacuation maps for the state.

Several guiding principles were established. From the outset, the focus is on tele-tsunamis, and not directly on local Hawaiian sources, or meteor impact origins (although both were obliquely considered). We consider the Aleutian–Alaska subduction zone the most dangerous source region (other zones were found to yield smaller tsunamis than comparable Aleutian earthquakes; i.e., even though there is a significant threat from Kamchatka—see Figs. 14 and 15 in “Appendix”—the potential threat from credible

Aleutian tsunamis is larger still). We consider ‘credible’ to mean that the physical parameters of the earthquake (faulting and slip) have been observed—or inferred from analysis—in prior Mw 9+ earthquakes (see Butler et al. 2016 for probabilistic analysis). Since the largest tsunami experienced in Hawai‘i is the 1946 event, we first validated our tsunami model forecasts with 1946 data, to link and corroborate knowledge of the earthquake with observed tsunami effects. We then model candidate Aleutian earthquake scenarios using two different tsunami codes to independently validate results—these methods comprise the NOAA operational code, SIFT, and the University of Hawai‘i research code, NEOWAVE (see “Appendix” for details). The effects of varying key parameters are explored to ascertain effects on tsunami amplitudes: fault areas, shallow and deep faulting, laterally varying distribution of slip on the faults, location along the arc, and earthquake seismic moment magnitude, Mw.

Tsunami forecasts were derived for 15 coastal regions of the State of Hawaii to determine which earthquake scenarios produced the largest tsunamis. Tsunami wave dispersion was not considered in this discovery phase, but has been included in subsequent evacuation mapping for the state. A map of the main Hawaiian Islands showing locations where simulations were run is shown in Fig. 3.

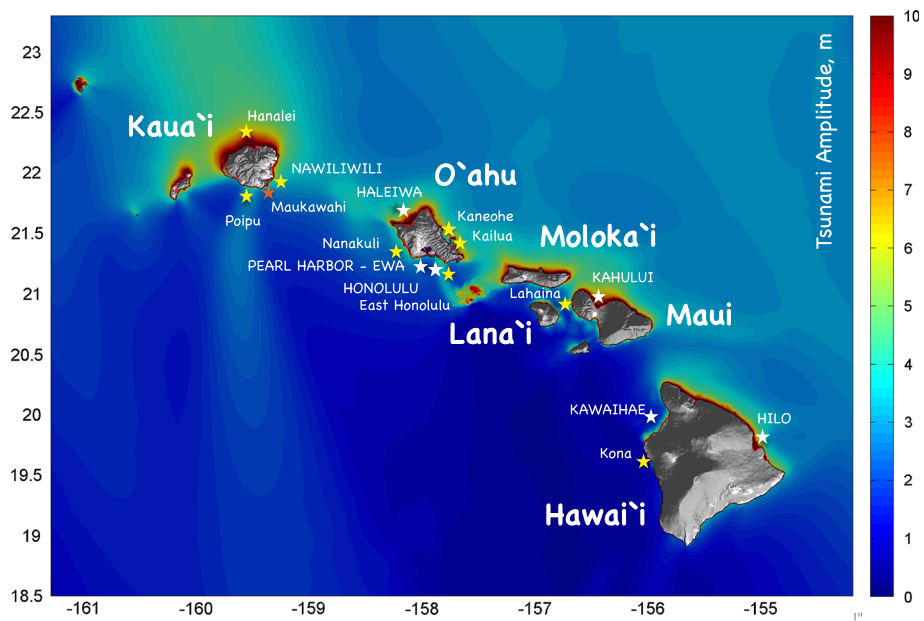


Fig. 3 The map of the Hawaiian Islands shows the coastal locations (filled stars) where tsunami forecasts were calculated for earthquake scenarios. Major islands are named. At the sites with white stars labeled in ALL CAPS, both SIFT/SIM and NEOWAVE methods were applied. At the other sites (yellow stars), only NEOWAVE was applied, since the SIFT/SIM models had not then been developed by NOAA at these harbors. Additionally, the paleotsunami site at Maukawahi cave on the southeastern Kaua‘i coast (Butler et al. 2014) is indicated by the orange star. The base map shows the maximum tsunami height in the ocean around the Islands for a Mw 9.25 scenario with 50-m fault slip near the trench and 20-m down dip. NB Open-ocean amplitudes approaching 5 m north of Kaua‘i and large resonance at the shallow Penguin Banks between O‘ahu and Moloka‘i

2 Earthquakes

2.1 The Aleutian tsunami of 1946

Butler (2012) reviewed the main characteristics of the 1946 Aleutian earthquake, for which the magnitude has been variously estimated from 7.1 to 9.3 (e.g., Johnson and Satake (1997). López and Okal (2006) derived a seismic moment of 8.5×10^{21} N-m from surface waves, equivalent to $M_w = 8.6$ with uncertainty $\geq \pm 0.1$. Length and width were determined from relocation of 1 year of aftershocks. The very slow rupture of the 1946 earthquake and limited instrumentation at the time preclude further resolution beyond average fault properties (López and Okal 2006). The fault length is stated as a conservative minimum, and the authors indicate that it could be 250 km; a width of 120 km was used in subsequent tsunami modeling (Okal and Hébert 2007) of 1946 tsunami data from the South Pacific. Johnson and Satake (1997) use a fault width of 145 km to model tide gauge data, but find little slip contribution in the deepest 50-km section. Tanioka and Seno (2001) modeled the event with a 40- to 60-km width in the shallowest section.

In order to calibrate our confidence in how big a tsunami will be in Hawai‘i from a great Aleutian earthquake, we first assess our knowledge of the crucial 1946 tsunami. The seismic moment M_0 or moment magnitude M_w of an earthquake does not uniquely define the fault, but rather determines the product of area A and displacement (slip) D on the fault though the formulae, $M_0 = \mu AD$ and $M_w = \frac{2}{3} \log_{10}(M_0) - 10.7$ (e.g., Aki 1966; Kanamori 1977), where μ is the rigid strength of the rock. For a given fault area, the tsunami amplitude scales directly with the slip (Okada 1985). Considering the uncertain trade-off between fault area and slip, we must consider a range of possible models for the 1946 event keyed to the magnitude M_w . This serves as a proxy for the real situation, where the first alert of a great tsunami comes from seismic data in the form of the moment magnitude. We consider a range of earthquake faults and slips for the 1946 event using the subfault framework of SIFT/SIM (see “Appendix”), as illustrated in Figs. 4, 16, 17, and 18. Tsunami amplitudes measured at eight sites in the Hawaiian Islands, 12 sites along the west coast of North America, and two sites in Samoa were compared with SIFT/SIM forecast model results. By calculating the geometric mean over the forecast/observed tsunami amplitude ratios for the data set, the fit to an M_w 8.6 earthquake can be judged. Table 1 summarizes fits for the various scenarios. As recognized in prior studies (e.g., Johnson and Satake 1997; Tanioka and Seno 2001), a preponderance of shallow faulting improves the overall fit to the data. These results were replicated using NEOWAVE for northwest O‘ahu data with similar conclusions. The Hawai‘i data are consistent with the Okal and Hébert (2007) South Pacific data set and the López and Okal (2006) seismic data. The results indicate that a moment magnitude of M_w 8.6 ± 0.1 is consistent with both the Hawai‘i and west coast data from 1946. This validation of consistency between the 1946 earthquake moment and the tsunami record is also corroborated by earthquake and tsunami data for the recent 2010 Chile (M_w 8.8) and 2011 Tohoku (M_w 9.1) events (see “Appendix”).

2.2 Aleutian model parameterization

We cannot simply define the earthquake capable of generating the largest tsunami by choosing an arbitrarily large seismic moment. Both the extent and distribution of faulting, and the amount and distribution of displacement at the seafloor need to be physically

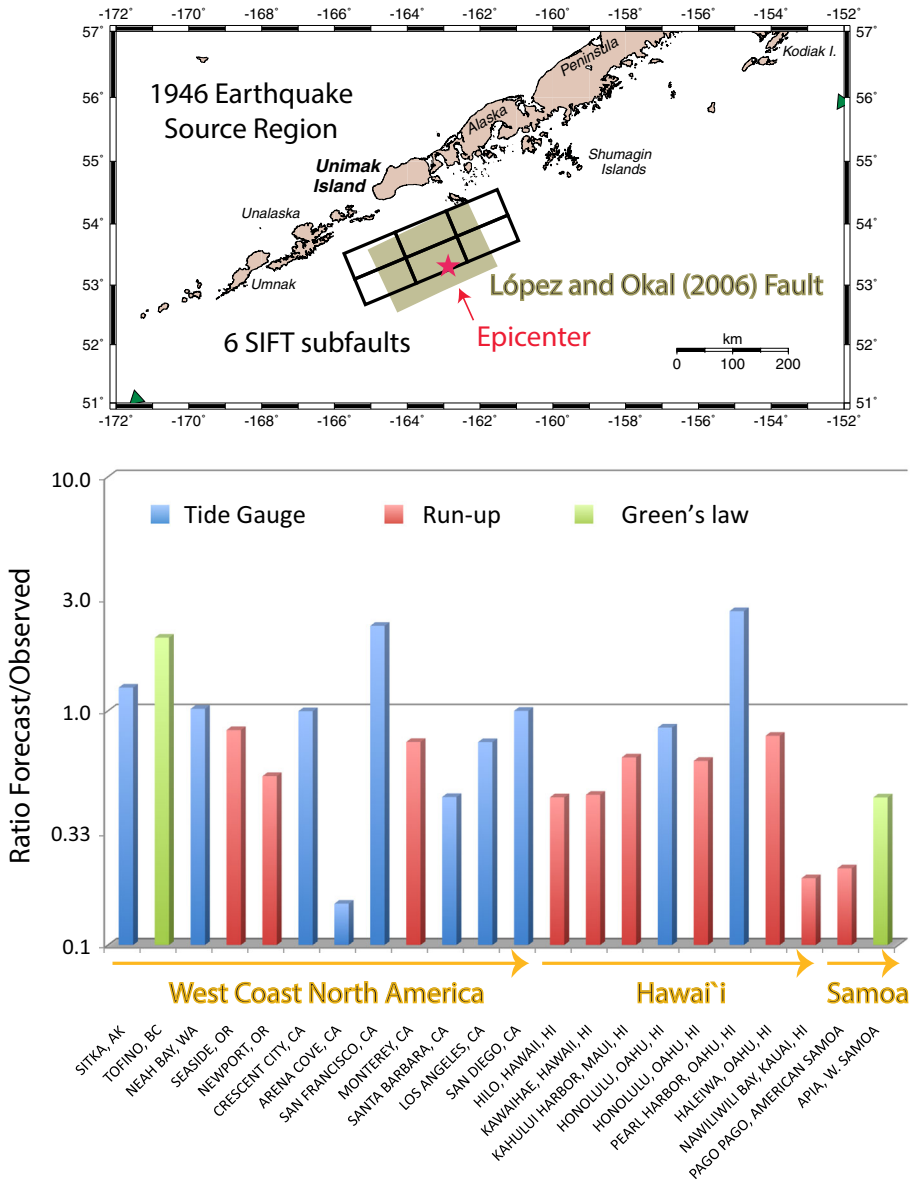


Fig. 4 The upper panel shows the location of the 1946 tsunami earthquake analyzed by López and Okal (2006) and Okal and Hébert (2007), who estimated 8–9 m of average slip over the 1946 fault. Their fault is approximated by sets of SIFT subfaults, encompassing west, east, central, shallow, and combined ruptures. In each case, the area and slip were adjusted to yield a constant moment magnitude of Mw 8.6 for which SIFT/SIM models were forecast. The tsunami data set includes all US measurements from tide gauges, observed run-up, or coastal amplitudes calculated via Green’s law. The ratio of the forecast value to the observed is plotted in the lower panel. In this example, all six SIFT subfaults, with fault slip = 7.4 m for a Mw 8.6 earthquake, were jointly forecast. Note that in this instantiation, the forecast amplitude for the 1946 event is too small compared with the observed data. However, other instantiations for a Mw 8.6 event fit better or are too large (see Figs. 16, 17, 18). Overall, the geometric mean of the models (Table 1) indicates that within the bounds of uncertainty, the tsunami measurements from 1946 using the model of López and Okal (2006) are consistent with Mw 8.6 ± 0.1

realizable. In determining these bounds, we use prior Mw 9.0+ events of the past 100 years as a guide.

The 1960 Chile earthquake (Mw 9.55) exhibited the largest average fault displacement overall, though estimates vary. Kanamori and Cipar (1974) estimated about 24-m slip using a larger rigidity of 7 (in units 10^{10} Pa), appropriate for deeper rupture than acknowledged today for these shallow megathrust events (Kanamori personal communication 2011). Using a rigidity of 4.4 appropriate for the Preliminary Reference Earth Model (PREM) (Dziewonski and Anderson 1981), a slip of 38 m is derived. Trade-offs in uncertainties in fault dip, depth, and area suggest a fault slip between 26 and 44 m, again assuming a standard rigidity of 4.4 rather than 6 (e.g., Cifuentes 1989). Geodetic methods, which account for only about one-fifth of the observed seismic moment, yield smaller values for the slip (Barrientos and Ward 1990). However, even for the smallest overall estimates for this earthquake, about 35 m of slip was observed in a segment of the earthquake equivalent to a Mw 9.0 event (Moreno et al. 2009). The value of 36 m in Butler (2012) is an average of several studies—35 to 38 m (Kanamori and Cipar 1974; Cifuentes 1989; Henry and Das 2001). Larger values of seismic moment for the main Chilean earthquake reported by Cifuentes and Silver (1989) are associated with greater uncertainty. The value ~ 35 m is used here, with an estimated uncertainty of about 5 m.

The 2004 Sumatra–Andaman earthquake (Mw 9.3) has the longest fault rupture recorded at about 1450 km (e.g., Lay et al. 2005; Ammon et al. 2005). The 2011 Tohoku earthquake (Mw 9.1) was characterized by relatively short overall rupture and large 50-m shallow displacement near the trench (e.g., Lay et al. 2011; Yamazaki et al. 2011b, c). The 1964 Alaska earthquake (Mw 9.2) was notable in laterally varying slip characterized by alternating large and small displacement patches on the fault (e.g., Ichinose et al. 2007), whereas the 1952 Kamchatka earthquake was characterized by small shallow displacement near the trench, increasing with depth (Johnson and Satake 1999). The large, deeper fault displacement characteristic of Kamchatka has smaller seafloor effects, and the resultant tsunami is smaller. In selecting features to generalize the maximum credible earthquake, we assume that in an extreme case 2 of the 3 major influences—large average slip (35 m), long fault length (up to 1500 km), and large slip (50 m) near trench—may interact together to create credible, physically realizable earthquakes.

3 Tsunami scenarios

3.1 Aleutian models

The two regions adjacent to the 1946 earthquake (Fig. 1) have not experienced significant seismic slip historically (Butler 2012). Westward is a ~ 700 -km segment of the Eastern Aleutian subduction zone between the 1946 and 1957 tsunamigenic earthquakes (Fig. 2). The second lies east of the 1946 earthquake in the Shumagin Islands and west of the rupture of the great 1964 Alaska earthquake (Figs. 14, 15). This second region is comprised of a ~ 600 -km segment of the subduction zone including the area of the 1938 earthquake, which, though large (Mw 8.3), averaged only 2 m or less of slip (Butler 2012). The Shumagin-1938 region has a greater tsunami impact on the west coast of North America than in Hawai'i (e.g., Kirby et al. 2013). However, for a comparable magnitude and fault size, the tsunami forecast modeling herein shows that an Eastern Aleutian

scenario produces run-ups in Hawaii up to 5 times larger than the Shumagin-1938 segment, attributable to the geometry of the subduction zone with respect to Hawai'i.

The initial analyses tested 40 earthquake scenarios using the SIFT/SIM code to forecast tsunamis in Hawai'i and reported results from 19 scenarios (Butler 2014). These events included earthquakes with uniform 35-m slip in the Eastern Aleutians, and events extending outward from the Eastern Aleutians laterally westward, laterally eastward, and symmetrically in both directions. The effect of variable slip, keeping average fault slip at 35 m, was explored by enhancing slip to 50 m on the first tier of subfaults nearest the trench with 20 m of slip on the second tier of subfaults behind these. This event (Fig. 5, Mw 9.25ab) emulates the larger slip near the trench (i.e., shallower) seen in the 2011 Tohoku earthquake. A series of tsunami models of earthquakes centered on the East Aleutians were also evaluated, emphasizing the symmetry of the subduction zone geometry in focusing tsunami energy toward Hawai'i (e.g., Fig. 5, Mw 9.43). The rupture of the East Aleutian segment through the region of the 1957 earthquake in the central Aleutians is simulated by a 1200-km-long fault (Fig. 4, Mw 9.45). To construct even larger earthquakes, up to Mw 9.6 with 35-m uniform slip, the earthquake fault models were extended

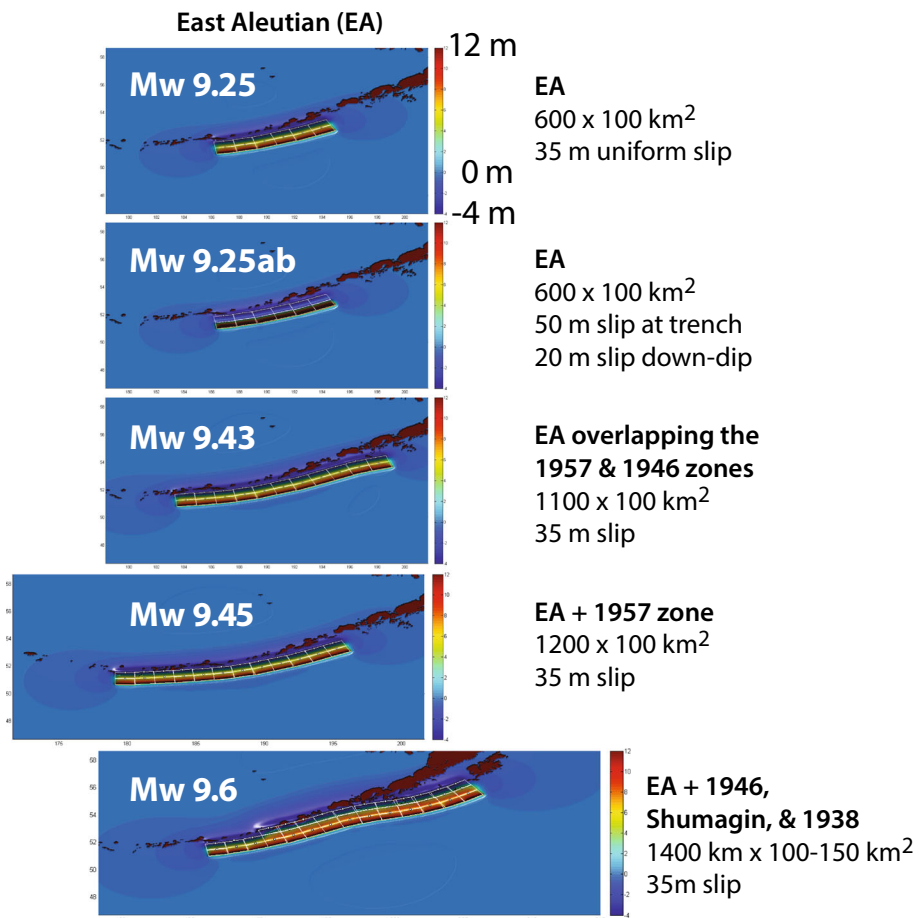


Fig. 5 The source extents of the great Aleutian earthquakes used to generate tsunami forecasts for Hawai'i

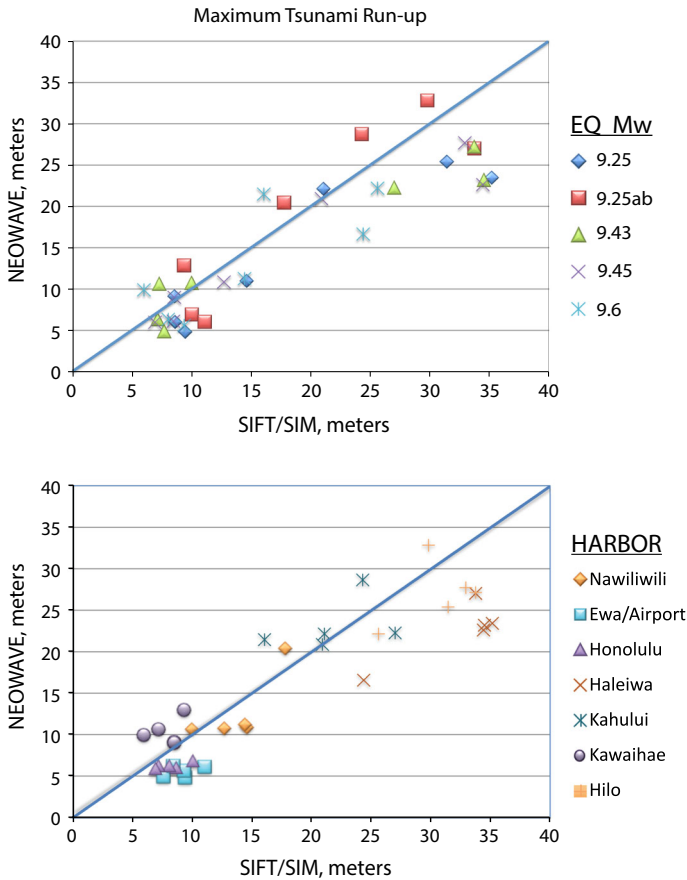


Fig. 6 Tsunami forecast run-up results compared between NEOWAVE and SIFT/SIM simulations where both forecast methods were applied: (*upper panel*) Aleutian earthquake sources (Fig. 5) and (*lower panel*) Hawaiian harbors (Fig. 3). The RMS error relative to the *plotted line* with unit slope is 5 m. Although both methods yield comparable results, substantial differences are apparent. NEOWAVE gives larger run-ups for the “shorter period” Mw 9.25ab earthquake (e.g., Fig. 12) with predominant slip near the trench, whereas the Haleiwa, Hilo, and Ewa/Pearl harbors produce generally larger run-ups (by ~5 m) from SIFT/SIM for most other events

from the Eastern Aleutians through the region of the 1946 earthquake to include rupture of the Shumagin-1938 segment within the same event. This largest event is 1400 km long, widening from 100 km in the west to 150 km in the east (Fig. 4, Mw 9.6), comparable in area to the great Sumatra–Andaman earthquake of 2004 (e.g., Lay et al. 2005). Details of the earthquake scenarios are listed in Table 2. Each of the five earthquake scenarios in Fig. 4 that generated the largest inundations and run-ups in the Hawaiian Islands was subjected to further model validation and testing using the University of Hawai‘i NEOWAVE computer code. Model validation by both SIFT/SIM and NEOWAVE used the same earthquake scenarios for each of seven Hawaiian harbors (Fig. 3).

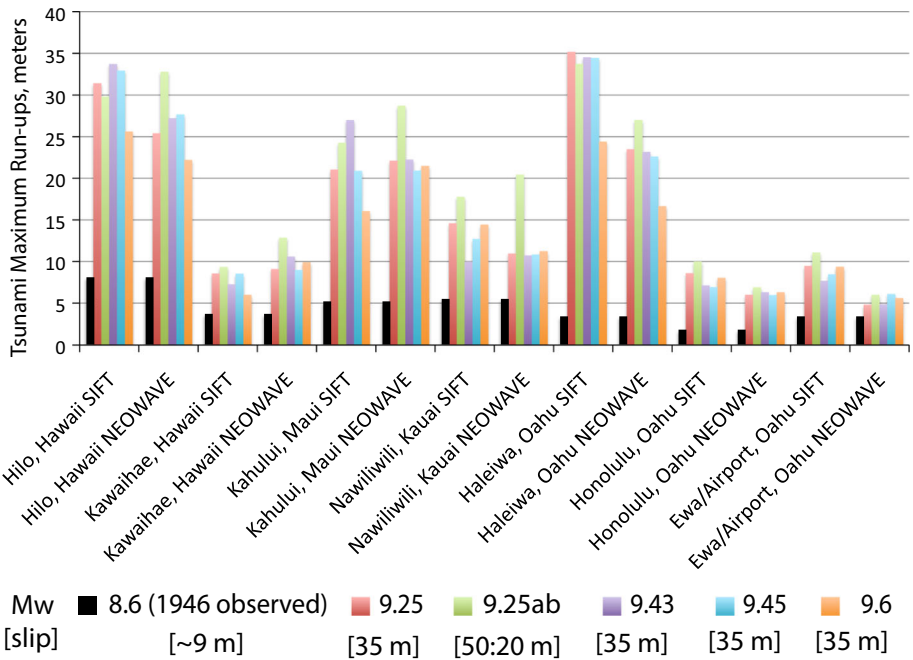


Fig. 7 Maximum tsunami run-ups (m) show paired NEOWAVE and SIFT/SIM models of 5 large Mw earthquakes in the Aleutians. The observed, historic maximum tsunami run-ups from the Mw 8.6 Aleutian earthquake of 1946 are indicated in *black* for seven Hawaiian harbors (run-up data from National Centers for Environmental Information); the mean fault slip in 1946 was estimated by Okal and Hébert (2007). Modeled earthquake fault slip is uniform, except for 9.25ab, where there is 50 m near the trench and 20-m down dip. Main points are: (1) 9.25ab is biggest at most sites, (2) 9.6 is generally smaller than other runs, especially for Hilo, Kawaihae, Kahului, and Haleiwa, where it is smaller than ALL other runs, (3) at Hilo and Haleiwa, 9.6 is smaller than all other runs (except 1946) for both SIFT and NEOWAVE, and (4) 9.6 is smaller than 9.25ab in every case

3.2 Tsunami model validations

Results from the two tsunami forecast methods are compared and contrasted in Figs. 6, 7, and 8, where identical earthquake source models were used to generate forecasts. Note that in principle, the results should not be expected to be identical, since the computational methods, digital bathymetry and topography data sets, model gridding assumptions, etc. differ. Further, whereas SIFT/SIM forecasts are available typically within ½ h (due to pre-computed propagation forecasts), the NEOWAVE forecast runs take up to 2 weeks to complete. These differences also reflect available knowledge in the rapid decision making at an operational level at the Pacific Tsunami Warning Center (PTWC) versus a university research setting.

A quantitative measure for comparing NEOWAVE and SIFT/SIM is the maximum run-up forecast in a harbor. This value is easily measured and specific to each harbor. The extent of inundation area, however, is the desired outcome related more directly to tsunami evacuation maps. Although qualitative maps are produced by the SIFT/SIM codes, specific measures of inundation area are not readily available from the operational codes accessed at PTWC. Further, the local small-scale grids are not identical between SIFT/SIM and

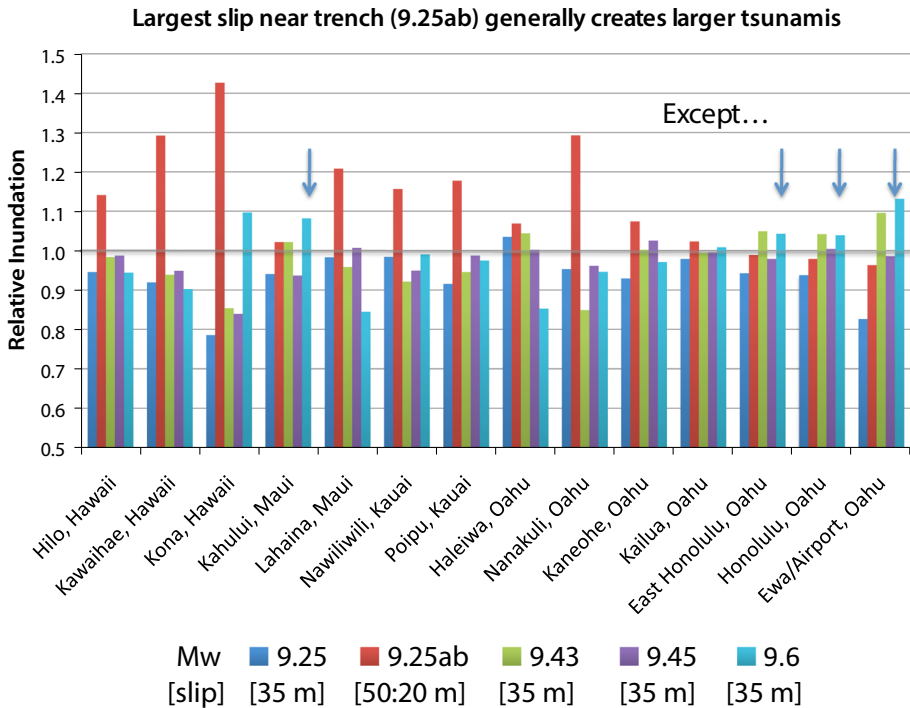


Fig. 8 The relative inundation area for NEOWAVE model runs of 5 large Mw Aleutian earthquakes. Fault slip is noted as uniform, except for 9.25ab, where there is 50 m near the trench and 20-m down dip. In most cases, large slip near the trench leads to the largest inundations in Hawai‘i. However, the south O‘ahu coast and Kahului, Maui, both forecast largest inundations (blue arrows) from earthquakes characterized by extreme fault length: Mw 9.6 (1400 km) and Mw 9.43 (1000 km)

NEOWAVE. Whereas this can still accommodate measuring maximum run-up, measures of inundation area become qualitative comparisons of maps. Therefore, the initial validation focused quantitatively on maximum run-up, and qualitatively on comparing maps.

The SIFT/SIM and NEOWAVE forecasts for maximum run-ups in 7 Hawaiian harbors are compared in Fig. 6. The comparison between SIFT/SIM and NEOWAVE is generally good and consistent with a clear trend along the line representing the same outcome. Large run-ups and smaller run-ups are similarly and consistently expressed by both NEOWAVE and SIFT. Nonetheless, for individual values there are significant excursions from unity. For instance, SIFT/SIMs show run-ups of 30–35 m where NEOWAVE has values of about 25 m. SIFT/SIM shows generally larger run-ups (more data lie to the right of the line). NEOWAVE gives generally larger run-ups for the Mw 9.25ab earthquake. The overall variation expressed as the root-mean-squared difference is 5 m. Therefore, overall the SIFT/SIM maximum run-ups vary by about 5 m from the NEOWAVE run-ups, for these very large earthquakes as forecast in Hawai‘i.

Maximum run-up results are compared by harbor region in Fig. 7, together with the observed maximum run-ups from the 1946 tsunami, which are dwarfed by 2–10 times larger forecasts for Mw 9+ events. The overall comparison between NEOWAVE and SIFT/SIM is qualitatively very good. Largest run-ups are observed at Hilo, Kahului, and Haleiwa, where harbor embayment resonance amplifies the tsunami (e.g., Mungler and

Cheung 2008). The largest differences are observed in Haleiwa, where SIFT/SIM forecasts significantly larger run-ups. For the other harbors, the two forecast methods give similar results. Nonetheless, the trend observed in Fig. 7 is again apparent—the Mw 9.25ab event with 50-m slip near the trench stands out for NEOWAVE. This is significant. For SIFT/SIM, there are diverse earthquake scenarios that give comparable maximum run-ups. However, the NEOWAVE forecasts indicate that the large slip near the trench is a critical factor influencing the maximum run-ups in Hawai'i and gives direction for reviewing maximum inundation scenarios.

The lack of a trend in Fig. 7 is striking: Earthquakes with larger fault areas do not systematically produce larger tsunamis. Although the earthquake magnitude and fault area vary by more than a factor of three, the maximum run-up remains relatively constant. For a uniform 35 m of slip at the earthquake source, the same initial deformation of the seafloor sets the initial tsunami amplitude (e.g., Okada 1985). For these very large events (≥ 600 km length), increasing the fault area qualitatively extends the breadth of the tsunami, but does not substantially affect its initial height. In fact, for harbors shown in Fig. 7 with the largest run-ups (Hilo, Kahului, Haleiwa) a 9.6 magnitude earthquake with uniform 35-m slip produces smaller run-up than do 9.25, 9.43, and 9.45 magnitude earthquakes with similar 35-m slip. The explanation for this effective maximum tsunami amplitude is explored in Sect. 3.5.

3.3 Tsunami inundations for the earthquake scenarios

In the initial analysis, the maximum run-up—from anywhere within each harbor grid—served as the principal quantitative measure, with qualitative estimates of inundation based on maps. For NEOWAVE, we have access to the output inundation data and can define the inundation area within a grid resolution of about 9 m. Since the inundation forecast has the greatest merit for differentiating earthquake scenarios, inundation area was measured for each site–scenario pair, for direct comparison of different earthquake scenarios at a common site. The earthquake scenarios were then tested at 8 additional coastal locations (Fig. 3) in the Islands—Hanalei and Po'ipu, Kaua'i; Nanakuli, Kaneohe, Kailua, and East Honolulu, O'ahu; Lahaina, Maui; and Kona, Hawai'i—to confirm the tsunami forecast trends observed previously. For each of these sites, all five earthquake scenarios were considered to strengthen the case for the largest Aleutian tsunami that may impact the Islands. Two scenarios emerged giving the largest tsunami forecasts: An earthquake contained within the Eastern Aleutians with largest slip near the subduction trench (Mw 9.25ab) and a larger event (Mw 9.6) with uniform faulting extending 1400 km northeast toward Kodiak Island.

Hanalei on Kaua'i experienced among the largest run-ups during the 1946 tsunami. The forecast for Hanalei showed the largest run-up for sites considered in the Hawaiian Islands from the Mw 9.25 Eastern Aleutian earthquake source—more than 40 m on a steep cliff west of Hanalei. However, other forecast scenarios could not be successfully completed for Hanalei, as the steepness of the gradient at the cliff face required fine tuning of the time-step in the computation not attempted in this analysis.

In parallel with this study, Butler et al. (2014) analyzed and dated the paleotsunami site in the Makauwahi sinkhole on the southeastern coast of Kaua'i between Po'ipu and Nawiliwili harbor (orange star in Fig. 3), positing evidence for a great tsunami there in the sixteenth century. At this site, which is 100 m from the beach and at an elevation of 7.2 m, tsunami forecast modeling was employed using NEOWAVE and high-resolution LiDAR data. This analysis utilized the same set of earthquake sources as this study, augmented

with additional sites in Kamchatka, Western Aleutians, and the Alaska Peninsula regions. Results indicate that an Eastern Aleutian earthquake of Mw 9.25 or greater is necessary to inundate the site. See Butler et al. (2014) for details and further discussion.

The normalized inundation for each of the 15 sites (7 initial + 7 new, excluding Hanalei) is plotted in Fig. 8. Inundation at each site is scaled by the mean of the inundations forecast from the five scenarios. Note that largest inundations flooding the harbor valleys do *not* necessarily correspond with maximum run-up, which often occur at steeper slopes. For most of the sites in Hawai‘i, the Mw 9.25ab event produces the largest inundations. However, for Kahului, Maui and Honolulu/Ewa, O‘ahu, the Mw 9.6 scenario produces larger inundations (with inundations from the 1100-km-long Mw 9.43 event comparable in Honolulu). Nonetheless, examples wherein a larger earthquake does not lead to larger inundations are also evident in Fig. 8. This effect is most conspicuous for Lahaina, Maui, Haleiwa, O‘ahu, and Hilo, Hawai‘i, but is a general observation in the inundations forecast among many of the events. Nonetheless, some incremental adjustments in the fault area do not follow this same trend. For example, increasing the eastward length *and* width of the East Aleutian fault does not yield greater inundations in Hilo, but increasing the fault length alone does (see next section).

Finally, for the O‘ahu communities of Kailua and Hawai‘i Kai, the tsunami inundations from these great tsunamis would top the barrier sandbars at the beachfront, flooding the interior villages—a disaster not experienced historically. It may be noted that O‘ahu’s main power plant is located at Kahe Point within the Nanakuli grid. Its current elevation is about 7.3 m, which is about double the prior local run-ups observed from the 1946 tsunami (3.7 m) and 1957 tsunami (3.4 m). For the Mw 9.25ab event shown in Fig. 5, run-ups exceed 15 m and the site is inundated. The other scenarios show smaller run-ups that reach or exceed the power plant’s elevation, and threaten significant inundation.

3.4 Effects of lateral variation in forcing

Earthquake scenarios were considered exploring (1) the effect of laterally varying the slip along the fault and (2) whether small perturbations in the length (from 600 to 700 km) and width (from 100 to 125 km or more) of faulting within the Eastern Aleutians may yield larger tsunami forecasts. For lateral variation in fault slip, five scenarios were tested (Fig. 9) in five harbors with significantly different inundation characteristics—Honolulu, Haleiwa, Hilo, Kahului, and Nawiliwili (Fig. 3). The relative inundation results are shown in Fig. 9, with slip varying significantly (stepwise between 20 and 50 m, averaging at 35 m overall) along 100-km segments. Compared to a model with uniform slip of 35 m, the variability in tsunami inundation forecasts within each harbor for each scenario is small, generally less than 5%. Figure 9 also compares the inundation maps for Honolulu for two cases, confirming the effect. This result indicates that for the giant Aleutian earthquakes being considered, substantial variations of slip along the length of the fault (as observed in the 1964 Alaska earthquake source, e.g., Johnson et al. 1996; Ichinose et al. 2007) do not significantly influence the inundation pattern relative to the uniform-slip models at these tele-tsunami distances. Close to the source, such lateral variation will be magnified in proximity, but with Hawai‘i at about 3500 km from the earthquake, the tsunami wave variations generated merge together and approximate the averaged case.

This is not the case in varying the slip from the trench down dip—changes in slip from 50- to 20-m down dip has a very large effect on the tsunami, seen in the Mw 9.25ab scenario compared with others. However, making the earthquake bigger simply by increasing the fault width (e.g., from 100 to 125 km) by adding deeper subfault tiers to the

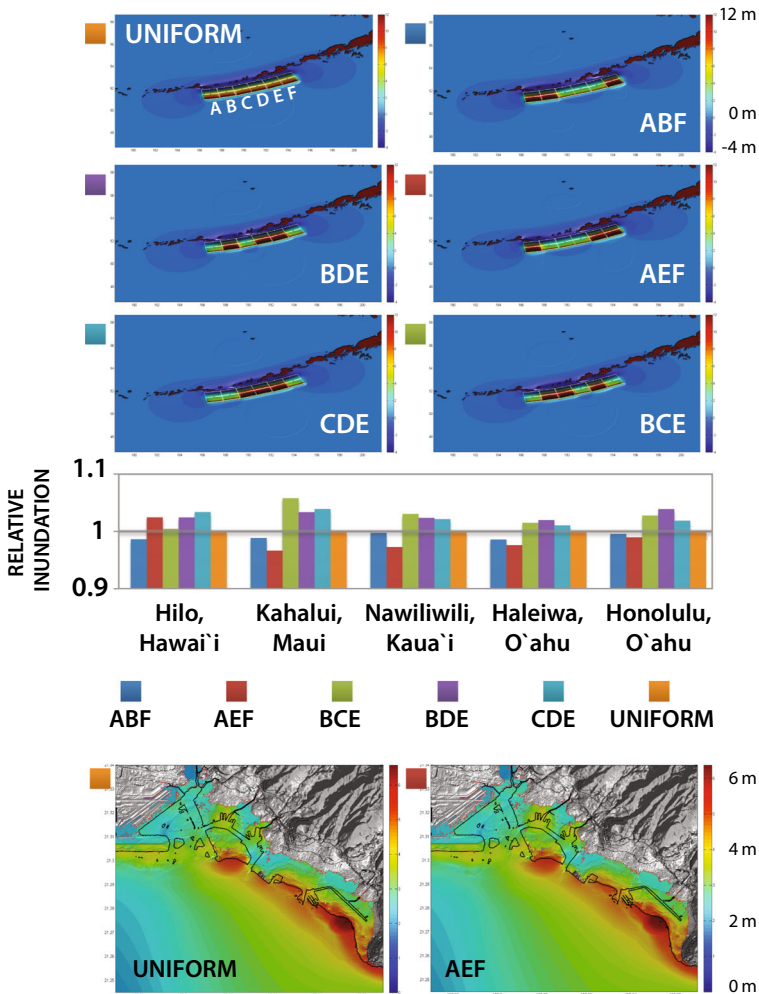


Fig. 9 Laterally varying slip models are analyzed with respect to tsunami forecasts for the Hawaiian Islands. The *top-left* panel shows the canonical Mw 9.25 with 35 m of uniform slip on all fault sub-segments, labeled A through F along strike. The initial, ocean tsunami amplitude is contoured in meters. The remaining five *upper panels* show non-uniform slip along strike, wherein lettered segments have 50-m slip and 20-m slip otherwise. The total average slip in each panel is 35 m, and all events are Mw 9.25. The *center panel* shows the relative inundation in five harbors (Fig. 3) for laterally varying event. *NB* the relative inundation varies by <5%. The bottom panel presents the inundation for Honolulu from the harbor to Waikiki, for the uniform-slip case (*left*) and one example (*right*) for a laterally varying slip at the source. *NB* although the relative variation of slip along the strike is extreme—alternately 50 m to 20 m to 50 m—there is little evidence of any effect in Honolulu. Similarly, the middle panels indicate similarly minor influences at other Hawaiian harbors

model framework does *not* in general increase the tsunami inundation and can decrease the maximum run-up. Rather, adding width changes the breadth of the tsunami but not its initial amplitude. By contrast, extending the Eastern Aleutian fault length from 600 to 700 km (extending eastward) and keeping the width at 100 km (Mw 9.29ab) does increase the inundation forecast at Hilo (Fig. 10). However, as Hilo is the most eastward harbor in

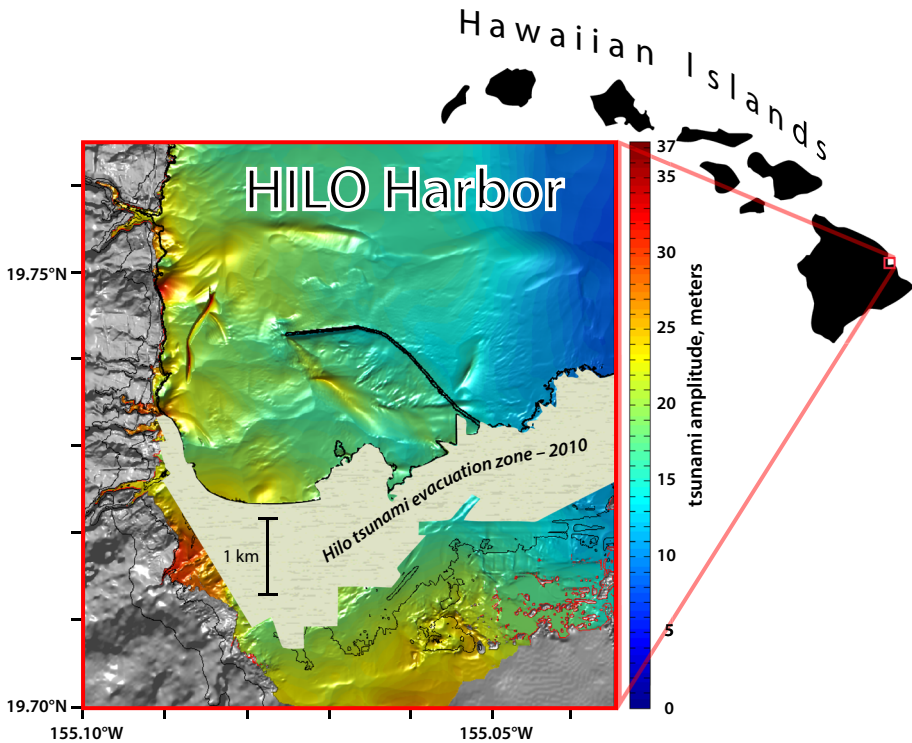


Fig. 10 Hilo Harbor—which experienced great tsunami disasters in the twentieth century—is shown in relation to the Hawaiian Islands. The tsunami evacuation zone based on historic tsunamis (cream textured, ca. 2010) is dwarfed by a great Aleutian tsunami (colored zone, amplitudes noted in meters) that extends >2-km inland. The earthquake scenario shown is Mw 9.29ab in Fig. 13

Hawai'i the eastward increase in the fault length also reduces the proximal tsunami propagation distance, which might contribute to the increased inundation forecast. Careful reflection on the earthquake faulting factors contributing to inundations—area, width, slip, depth of faulting, water depth, and the geometry of the tsunamigenesis—must be considered in assessing potential tsunamigenic inundation.

3.5 Tsunami wavelength

The wavelength of the tsunami clearly has an effect on the resulting coastal inundation. The size of the earthquake source (fault area) has a direct influence on the wavelength of the tsunami. Resonance phenomena observed in tsunami amplitudes in Hawaiian harbors have been related to coastal response characteristics depending on the geometry, shape, and bathymetry profile (e.g., Munger and Cheung 2008) and its interaction with the spectral content of the tsunami. In the present analysis, it is clear that the tsunami wavelength has an influence on the run-up and inundation, and must be a consideration in determining the extent of evacuation zones. The key phenomenon observed in the joint forecasts is that increasing earthquake magnitude does not, by itself, lead to a larger tsunami. Rather, both the amount of slip and the fault area contribute in different measures.

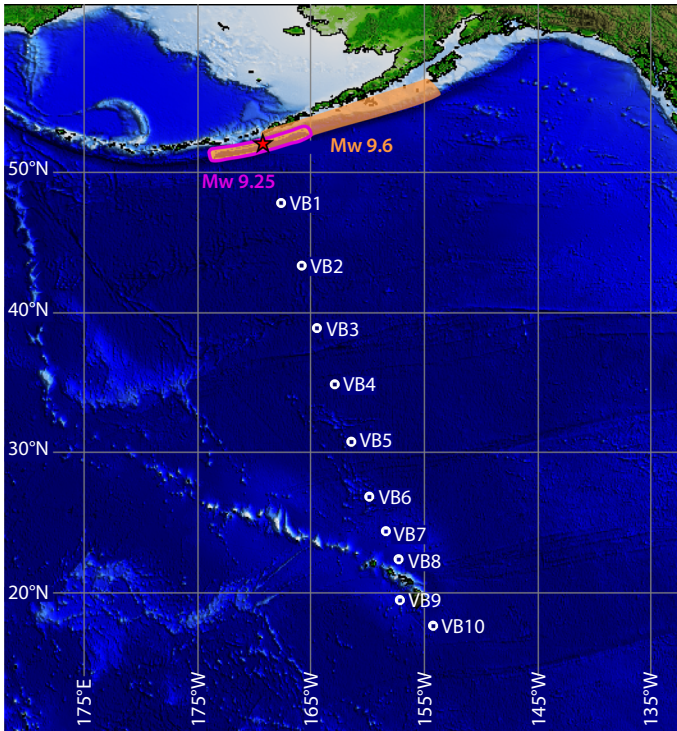


Fig. 11 Extreme earthquakes and locations of Virtual Buoys (VB). The Mw 9.25 Eastern Aleutian earthquake is circled in magenta, and the Mw 9.6 earthquake includes the Eastern Aleutians and extends up to Kodiak Island. Open-ocean tsunami amplitudes and waveforms are shown in Fig. 11 annotated VB by number

By the Okada (1985) elastic relations, tsunami amplitudes are related directly to slip on the fault. However, doubling the fault area does *not* necessarily lead to tsunami amplitude increase, but does increase the amplitude of longer wavelength components of the tsunami. Since coastal resonances are excited by the spectral characteristic of the tsunami, to gain a more complete understanding of the range of inundations/run-up it is necessary to include *both* longer and shorter wavelength tsunamis, derived from the setting and characteristics of the earthquake.

At the coast the local effects of resonance are inextricably intertwined with the tsunami spectrum. To illustrate the situation clearly, we created a series of ‘virtual buoys’ aligned from the earthquake source region to Hawai‘i. The advantage gained is that the open-ocean waveform of the tsunami may be viewed as it evolves in propagation to the Islands, relatively free from coastal influences. The arrangement of the virtual buoys is shown in Fig. 11. We use as example the Mw 9.6 as representative of a large area source, whereas the Mw 9.25ab event creates a relatively shorter wavelength source. The difference in frequency/wavelength content of the two tsunamis is substantial (Fig. 12). The Mw 9.25ab and 9.6 events have maximum power at about 20- and 100-min period, respectively. At an open-ocean tsunami wave speed of about 0.25 km/s, the corresponding principle wavelengths are about 300 and 1500 km, respectively. With these long wavelengths, effects of

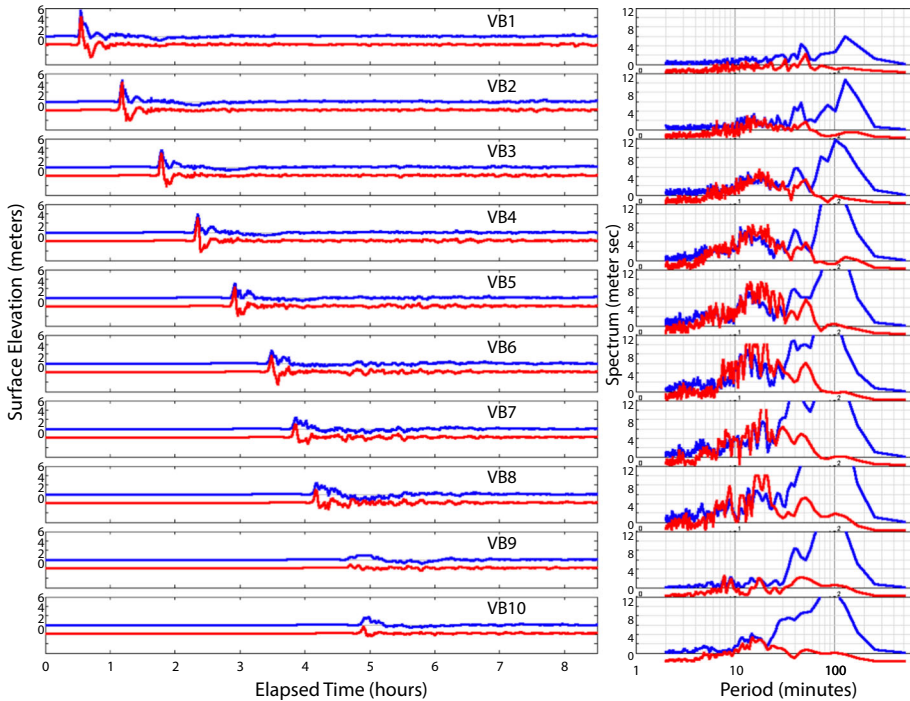


Fig. 12 *Left panel* shows tsunami waveform and amplitude in the open ocean at virtual buoy (VB) locations in Fig. 11. *Right panel* shows spectral content. *NB* the period is *minutes*. The *red* and *blue* curves are the Mw 9.25 and 9.6 events, respectively. Note that the Mw 9.6 event possesses abundantly more long period energy. The difference in frequency content for the two extreme events leads to differing coastal responses, and hence contrasting inundation patterns. Note also that VB9 and VB10 have already interacted with the coastal response of Hawai‘i

dispersion as the waves propagate through the deep ocean should be negligible (e.g., chapter 5 in Gill 1982). Each tsunami will interact differently in approaching and interacting with the coast. Although a simplification, this phenomenon is shown in Fig. 8, where sites on Maui and southern O‘ahu experience larger inundations from the longer wavelength tsunami, whereas most other sites respond more strongly to the shorter wavelength tsunami. Nonetheless, this points toward the necessity in using *both* longer and shorter wavelength tsunamis in our analysis.

3.6 Tsunamigenesis of maximum credible earthquakes

Two earthquake sources were selected and recommended to the Hawaii Emergency Management Agency for use in constructing new tsunami evacuation maps for the Hawaiian Islands. This recommendation was guided by (1) a systematic analysis of credible earthquake sources based on prior Mw 9.0+ events; (2) application of two independent, validated tsunami models to forecast inundation and run-up effects in Hawai‘i; (3) available historical documentation; and (4) paleotsunami evidence on Kaua‘i of a tsunamigenic Mw 9 event in the sixteenth century impacting Hawai‘i, analyzed in

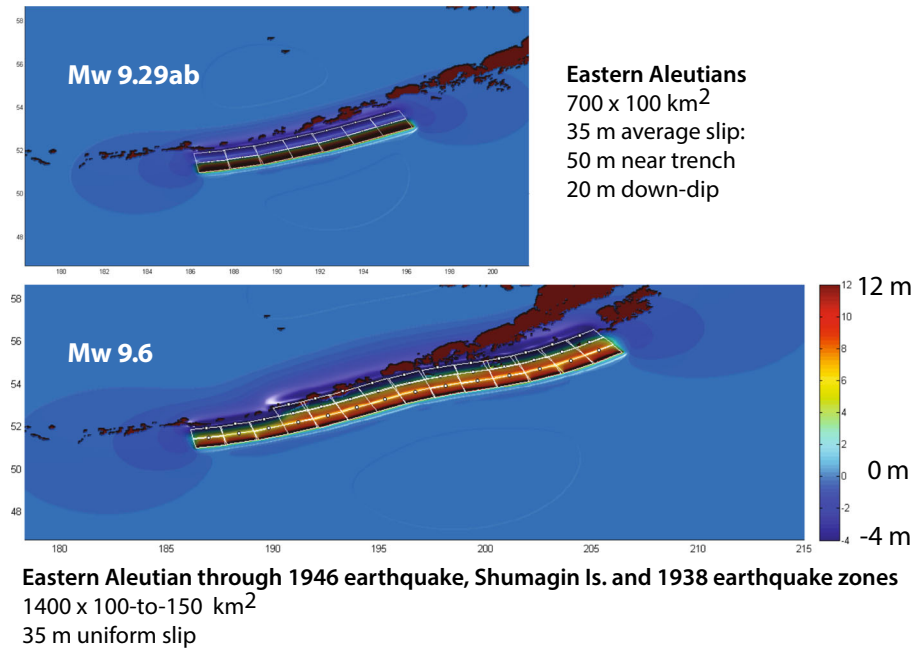


Fig. 13 The source extents and slip distributions of the two extreme Aleutian earthquakes forecasting the largest credible tsunamis in the Hawaiian Islands

conjunction with this study published independently (Butler *et al.* 2014). These two earthquake sources—each averaging 35 m of fault slip—are shown in Fig. 13 and include both a Mw 9.29ab event with extreme slip near the trench and a Mw 9.6 earthquake with extreme length. Either event would be catastrophic in its impact on the Islands. Both serve as input to further development of new tsunami evacuation maps.

4 Discussion

The State of Hawaii has experienced 225 deaths due to tsunamis since 1900 (National Centers for Environmental Information, NOAA 2016). All 49 other states combined have experienced 160 tsunami-related deaths since 1900. In Alaska alone, the local tsunamis from the 1964 Alaska earthquake caused 106 deaths. However, nearly all Hawaiian deaths were due to earthquakes more than 3500 km distant from the Islands. This is a unique situation, quite different from the local devastation of the 2011 Tohoku event. All of Hawai‘i’s coastline, population, and coastal infrastructure are vulnerable in a way not seen elsewhere in the USA.

The results of the analysis show that Mw 9.0+ earthquakes in the Aleutians have forecast tsunamis in Hawai‘i that substantially exceed current tsunami evacuation maps (ca. 2010) in 14 of the 15 coastal zones considered, the sole exception being the west (Kona) coast of the Big Island. Figure 10 shows the worst-case scenario for Hilo, which has been devastated by the historical tsunamis of 1946 and 1960 that had served as the

basis for existing tsunami evacuation maps. The potential inundation zone for an extreme Aleutian tsunami could more than double historic flooding. Significantly enhanced inundations are forecast on O‘ahu in Kailua and Hawaii Kai—where overtopping of the beach sand bar leads to extensive flooding—and at the Kaneohe Marine Base and the Kahe Power Plant. All of these effects are encompassed by the two earthquake scenarios that together produce the largest tsunami forecasts. These scenarios have been submitted to and accepted by Hawaii State Civil Defense for deriving new, extended ‘extreme’ tsunami evacuation zone maps for the State of Hawaii. Further, although this is a theoretical analysis, paleotsunami evidence on Kaua‘i corroborates the reality of such events in Hawai‘i’s past (Butler *et al.* 2014).

In as much as the focus of this analysis is to determine the largest Aleutian tsunami that may potentially impact Hawai‘i, could even larger earthquakes cause larger inundations? In principle, yes. However, a larger earthquake implies a larger seismic moment (greater energy), which in turn implies larger fault area and/or slip. We have seen that incrementally increasing the fault area can lead to increasing the tsunami run-up or inundation (e.g., Fig. 10), but that large increases in the length and width of the faulting do *not* correspondingly increase run-up/inundation (Figs. 7, 8). We have considered scenarios where there are extremes of 50-m slip, limited to near the shallow trench or along lateral portions of the fault length. However, in each case 35 m of average slip was maintained to be consistent with the greatest average slip observed in seismic data for the great Mw 9.55 Chilean earthquake of 1960—the largest earthquake ever recorded. Increasing the average slip along the entire fault to 40 or 50 m would increase tsunami amplitudes. Since sea floor deformation is directly proportional to slip on the fault (Okada 1985), increasing the average slip along the entire fault to 40 or 50 m would effectively increase the tsunami amplitudes at the source by about 15 or 45%, respectively. Although nonlinear effects must be considered, larger tsunamis in Hawai‘i would result. However, to make this assumption we must presume that the largest slip (~ 50 m for the 2011 Tohoku Japan earthquake) ever observed on a *portion* of a fault could occur as the average over the *entire* fault surface. Such an assumption is not yet warranted.

4.1 Summary

A detailed analysis is presented for determining the maximum credible earthquakes forecasting extreme tsunami run-up and inundation in the Hawaiian Islands. The purpose of the study is to provide guidance to the Hawaii Emergency Management Agency for new tsunami evacuation maps being re-drawn following the 2011 Tohoku disaster. Only tele-tsunami sources are considered, and after review the Aleutians pose the greatest threat to Hawai‘i. Hawaiian data are first modeled for the great 1946 tsunami to validate our ability to characterize the tsunami source, propagation, and response by the Hawaiian coasts. Two state-of-the-art tsunami forecast methods are jointly employed to validate the results. Wave diffraction and refraction effects create hazards on all coasts. Earthquake sources are parameterized by physical faulting characteristics observed in prior $M_w \geq 9$ earthquakes: utilizing extensive investigation of source locations, faulting areas, shallow-vs-deep and laterally varying distributions of fault slip, coastal resonance influences, and wavelength-dependent coastal responses. This methodology is focused primarily on distant tele-tsunamis impacting Hawai‘i.

Acknowledgements The work has greatly benefited by collaboration with the Pacific Tsunami Warning Center (PTWC). In particular, RB thanks PTWC for access to their SIFT/SIM tsunami codes for the analysis work. For their insightful discussions of tsunamis, we thank Gerard Fryer and Chip McCreery at PTWC and

Yefei Bai, Kwok Fai Cheung, and Yoshiki Yamazaki at the Hawai'i Tsunami Mapping Project (HTMP) at the University of Hawai'i (UH). We thank Yefei Bai and HTMP for providing access and expert assistance in using the NEOWAVE tsunami code for high-resolution tsunami forecast simulations. This work was supported in part by the Hawaii State Civil Defense (now Emergency Management Agency) and by the UH School of Ocean and Earth Science and Technology (SOEST). SOEST Contribution No. 9853, HIGP Contribution No. 2235.

Data statement Tsunami run-up and inundation data from the 1946 event are from the National Centers for Environmental Information, last accessed April 2016: (<https://www.ngdc.noaa.gov/nndc/struts/form?t=101650&s=166&d=166>). Earthquake parameters and subfault details used in this analysis are listed in Table 2. Digital bathymetry and topography data used in the tsunami forecasts are discussed and referenced in “Appendix.” Extensive inundation maps for Hawaiian harbors are found in Butler (2014).

Open Access This article is distributed under the terms of the Creative Commons Attribution 4.0 International License (<http://creativecommons.org/licenses/by/4.0/>), which permits unrestricted use, distribution, and reproduction in any medium, provided you give appropriate credit to the original author(s) and the source, provide a link to the Creative Commons license, and indicate if changes were made.

Glossary

Displacement	Amount of fault motion in meters same as Slip
Down dip	The deeper region of the dipping fault
Earthquake source mechanism	Fault parameters including area, strike, dip, rake, displacement, rock rigidity, area
Megathrust	Great earthquake with thrust mechanism, also a fault capable of a great earthquake
Mw	Magnitude of earthquake derived from its seismic moment
NEOWAVE	University of Hawai'i tsunami code
NOAA	National Oceanic and Atmospheric Administration
Paleotsunami	Pre-historic tsunami
PREM	Preliminary reference earth model
PTWC	Pacific Tsunami Warning Center
Richter scale	Historical magnitude scale no longer used, see Mw
SIFT/SIM	NOAA tsunami code
Slip	Amount of fault motion, in meters, same as displacement
Subfault	100 km × 50 km fault unit
Tele-tsunami	Tsunami that travels from a great distance, i.e., not locally generated
Tsunamigenic, tsunamigenesis	Tsunami producing
Virtual buoys	Open-ocean sites (within model framework) where the tsunami is measured

Appendix

Figs. 14, 15, 16, 17, 18.

Table 1 Fault models of the 1946 Aleutian earthquake for $M_w = 8.6$ where slip \times area = constant. Geometric means of SIFT forecast/observation (Figs. 4, 16, 17, 18) are shown for several geometric allotments of fault area for the earthquake

Fault area Segments	ALL	Center	West	East	Center shallow	West shallow	East shallow
All	0.7	1.0	0.8	0.8	1.6	1.0	1.1
Hawaii	0.6	0.7	0.7	0.7	1.5	1.3	1.4
Non-Hawaii	0.7	1.2	0.9	0.9	1.7	0.9	0.9

For a given fault area, ± 0.1 uncertainty of M_w corresponds to a factor of 0.7–1.4 in forecast/observation geometric means, which encompasses the full range of faulting scenarios

Table 2 Faulting parameters are shown for earthquakes discussed

Earthquake Mw	Uniform fault slip (m)	Region (Figs. 1, 4)	SIFT subfaults, fault length, and area ^a
Mw 9.25	35	East Aleutians	ac18–23ab 600 km, 60,000 km ²
Mw 9.25	35	Alaska Peninsula	ac26–31ab 600 km, 60,000 km ²
Mw 9.25	35	Quasi-1957	ac12–17ab 600 km, 60,000 km ²
Mw 9.25	35	Quasi-Kamchatka	ki2–7ab 600 km, 60,000 km ²
Mw 9.25ab (50–20 m)	50 (b), 20 (a) 35 average	East Aleutians	ac18–23ab 600 km, 60,000 km ²
Mw 9.29ab (50–20 m)	50 (b), 20 (a) 35 average	East Aleutians	ac18–24ab 700 km, 70,000 km ²
Mw 9.43	35	1957, East Aleutians, 1946, Shumagin	ac16–26ab 1100 km, 110,000 km ²
Mw 9.45	35	1957, East Aleutians	ac13–24ab 1200 km, 120,000 km ²
Mw 9.6	35	East Aleutian, 1946, Shumagin, 1938	ac18–31ab, ac21–31z 1400 km, 195,000 km ²

^a Each subfault has a unique identification code and corresponding location, fault geometry, and depth—see Gica et al. (2008) and its appendices. For example, ac18–23b refers to “Aleutian-Cascadia” subfaults 18 through 23, tier b (along the trench), which is 600 km long and 50 km wide. Tiers a, z, and y are subfaults successively further from the trench, and deeper. The fault width varies with the number of 50-km-wide subfault tiers incorporated in the earthquake. Earthquake Mw corresponds with a rigidity of 44 GPa for PREM. All events are modeled as pure thrust mechanisms

Computational method

We use NEOWAVE (Non-hydrostatic Evolution of Ocean Wave) of Yamazaki et al. (2009, 2011b) to model each tsunami from generation at the earthquake source to inundation at the coastline of Kaua‘i. The staggered finite difference model builds on the nonlinear shallow-water equations with a momentum conservation scheme to approximate breaking waves as bores or hydraulic jumps as in a finite volume model (e.g., Wei et al. 2006; Wu and Cheung 2008). The code accommodates up to five levels of two-way nested grids to describe processes of different time and spatial scales from the open ocean to the coast.

NEOWAVE has been validated against the benchmarks put forth by the National Tsunami Hazard Mitigation Program and the National Science Foundation and is approved by the National Ocean and Atmospheric Agency (NOAA) for use in tsunami inundation mapping (Yamazaki et al. 2012a). NEOWAVE has been validated with near and far-field measurements from the 2009 Samoa, 2010 Mentawai, 2010 Chile, 2011 Tohoku, 2012 Haida Gwaii, and the 2013 Santa Cruz Islands tsunamis (Lay et al. 2011a, b, 2013a, b; Roeber et al. 2010; Yamazaki and Cheung 2011; Yamazaki et al. 2011a, c, 2012b, 2013).

For calculation of tsunami forecasts for the Japanese and Pacific West Coasts, we used the SIFT (Short-term Inundation Forecast for Tsunamis) computer code (Titov and González 1997; Titov and Synolakis 1998; Titov et al. 2005; Gica et al. 2008; Tang et al. 2009;

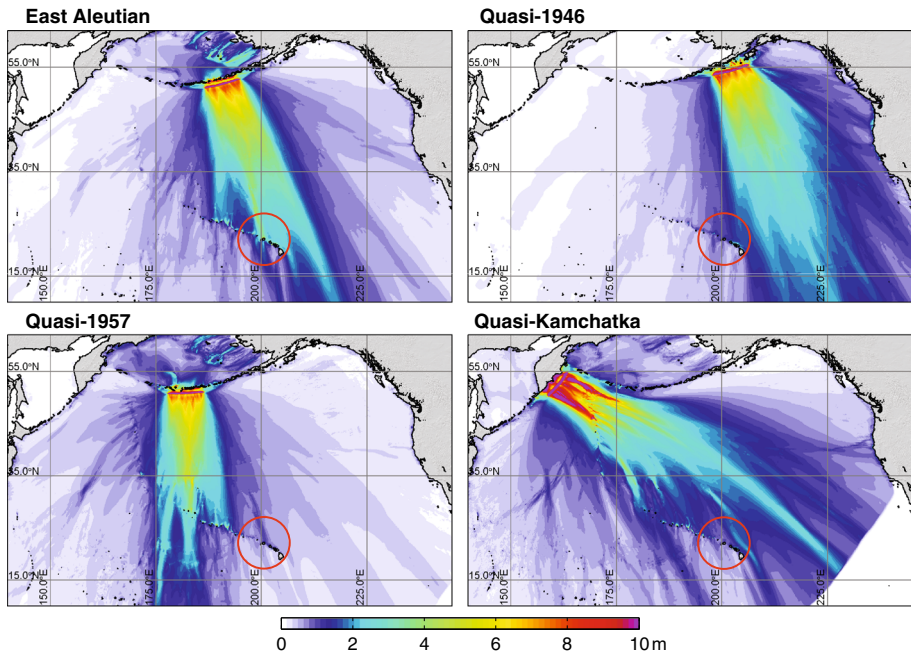


Fig. 14 Maximum tsunami amplitudes in meters are forecast using NEOWAVE for identical (size, fault slip) Mw 9.25 earthquakes: (*upper left*) the east Aleutians; (*upper right*) the Alaska Peninsula region extending eastward from the Shumagin Islands to the west of Kodiak Island; (*lower left*) a quasi-1957 event; and (*lower right*) a quasi-Kamchatka event. The *red circles* are centered on Kaua’i and encircle the Big Island. Note that only the Eastern Aleutian tsunami energy is directed primarily toward Hawai’i

references contain extensive method validations) of the NOAA. Complete inundation forecasts were computed using the NOAA Stand-by Inundation Models (SIMs) for 20 harbors along the Pacific Coast.

Whereas SIFT/SIM forecasts are limited to preselected harbor regions, the comprehensive digital elevation database of the University of Hawai’i permits NEOWAVE to forecast tsunami results along any Hawaiian coast. This is not unlimited, since the highest resolution (~3 m) LIDAR data are available only to 15-m elevation. Therefore, the very largest run-ups are computed with lesser resolution.

Digital elevation model

The National Geophysical Data Center (NGDC) ETOPO1 Global Relief Model at 1-arcmin resolution (Amante and Eakins 2009) is used for modeling Pacific basin-wide tsunami propagation. ETOPO1 has approximately 1850-m resolution near the Hawaiian Islands, where higher-resolution data sets are used. The majority of the offshore bathymetry is the 1.5-arcsec (46-m) resolution University of Hawai’i SOEST multibeam data and the gaps are filled by the 5-arcsec (154-m) US Geological Survey (USGS) I-2809 data set. The near-shore bathymetry source is the SHOALS (Scanning Hydrographic Operational Airborne LiDAR Survey) data set, which was procured by the US Army Corps of Engineers (USACE) between 1999 and 2004. The data extend from the shoreline to approximately

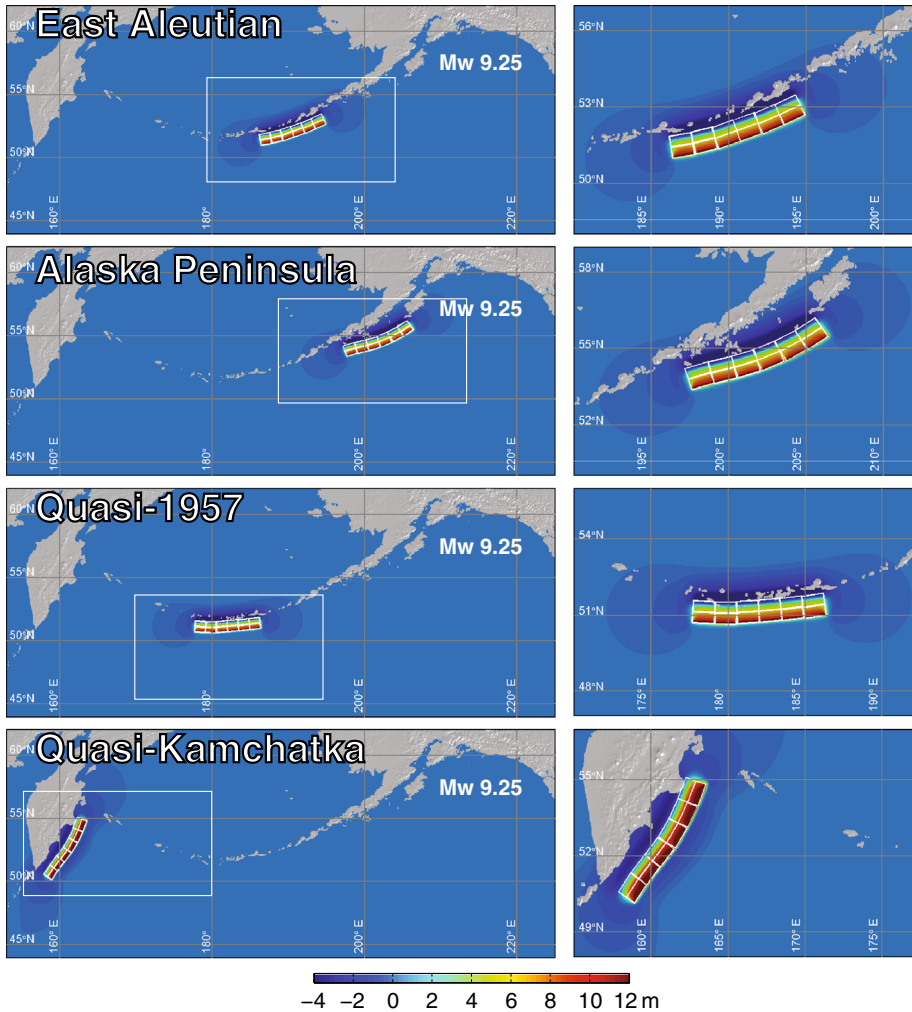


Fig. 15 The subfault locations and initial tsunami ocean amplitudes (in m) are shown for comparable Mw 9.25 earthquakes in Fig. 14 along the Kamchatka–Aleutian–Alaska arc. The tsunami forecast for the Eastern Aleutian event is most dangerous for the Hawaiian Islands

40-m water depth at 4-m horizontal resolution. Data from hydrographic surveys and nautical charts supplement the near-shore bathymetry, mostly inside harbors and marinas.

The topography is from the USGS 0.33 and 1-arcsec (10- and 30-m) digital elevation models, which include the SRTM (shuttle radar topography mission) data. LiDAR (light detection and ranging) topography data are used near the Kaua’i coastline with 1-m horizontal resolution extending from the shoreline to the 15-m elevation contour—the data for the north- and south-facing shores procured by USACE and Federal Emergency Management Agency, respectively.

This study implemented four levels of nested grids to model tsunami propagation across Pacific and inundation in Hawai’i. The level-1 grid at 2-arcmin resolution (~3000 m)

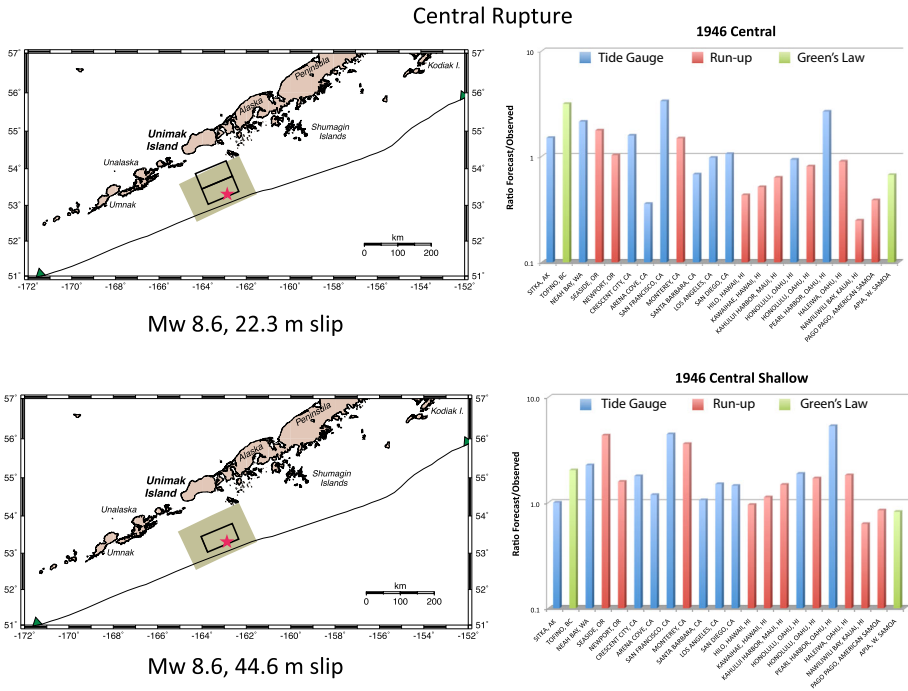


Fig. 16 Tsunami model results for rupture of central segments of 1946 faulting region for constant magnitude, $M_w = 8.6$

extends the North Pacific Ocean to describe tsunami generation and propagation. The level-2 grid at 15 arcsec (~ 463 m) and the level-3 grids at 3 arcsec (~ 90 m) resolve tsunami transformation around Hawaiian Islands and the Kaua'i Island, respectively. A level-4 grid at 0.3 arcsec (~ 9 m) is used for high resolution.

For the SIFT/SIM tsunami forecasts along the Pacific West Coast, the initial forecasts were pre-computed at 4-arcmin resolution in the open ocean and stored at 16-arcmin resolution. Nested grids are used in the SIMs to achieve successively greater detail (Tang et al. 2009): a regional grid of 2-arcmin (~ 3700 -m), intermediate grids of 12- to 18-arcsec (~ 370 - to 555-m) at the coast and elsewhere, and a harbor region grid of about 2-arcsec (~ 60 -m) resolution.

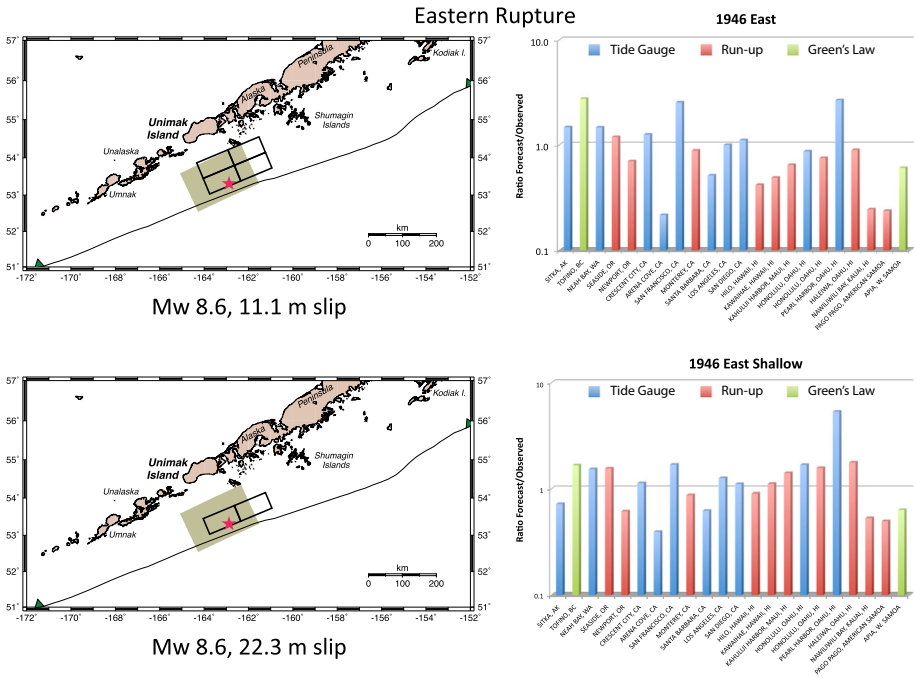


Fig. 17 Tsunami model results for rupture of eastern segments of 1946 faulting region for constant magnitude, $M_w = 8.6$

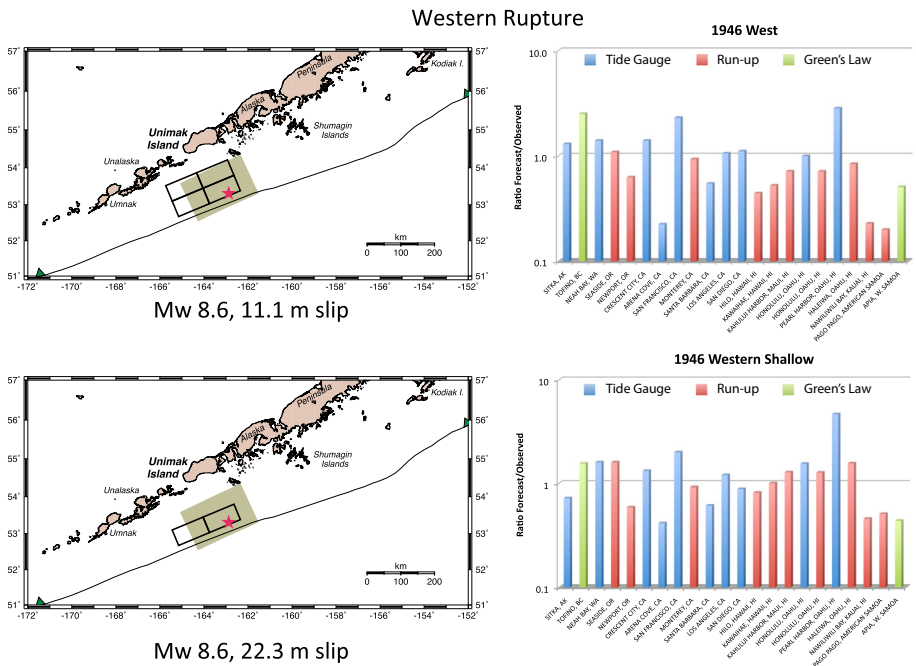


Fig. 18 Tsunami model results for rupture of western segments of 1946 faulting region for constant magnitude, $M_w = 8.6$

References

- Aki K (1966) Generation and propagation of G waves from the Niigata earthquake of June 16, 1964, Part 2: estimation of earthquake moment, released energy, and stress-strain drop from G wave spectrum. *Bull Earthq Res Inst Tokyo Univ* 44:73–88
- Amante C, Eakins BW (2009) ETOPO1 1 Arc-minute global relief model: procedures, data sources and analysis. NOAA Technical Memorandum, NESDIS NGDC-24
- Ammon CJ, Ji C, Thio H-K, Robinson D, Ni S, Hjorleifsdottir V, Kanamori H, Lay T, Das S, Helmberger DV, Ichinose G, Polet J, Wald D (2005) Rupture process of the great 2004 Sumatra–Andaman earthquake. *Science* 308:1133–1139
- Barrientos SE, Ward SN (1990) The 1960 Chile earthquake; inversion for slip distribution from surface deformation. *Geophys J Int* 103:589–598
- Butler R (2012) Re-examination of the potential for great earthquakes along the Aleutian island arc with implication for tsunamis in Hawai'i. *Seismol Res Lett* 83(1):30–39. doi:10.1785/gssrl.83.1
- Butler R (2014) Great Aleutian Earthquakes. Hawai'i Institute of Geophysics and Planetology, peer-reviewed report HIGP-2014-1
- Butler R, Burney D, Walsh D (2014) Paleotsunami evidence on Kaua'i and numerical modeling of a great Aleutian tsunami. *Geophys Res Lett* 41(19):6795–6802
- Butler R, Frazer LN, Templeton WJ (2016) Bayesian probabilities for Mw 9.0 + earthquakes in the Aleutian Islands from a regionally scaled global rate. *J Geophys Res Solid Earth* 121(B5):3586–3608. doi:10.1002/2016JB012861
- Cifuentes IL (1989) The 1960 Chilean earthquakes. *J Geophys Res* 94:665–680
- Cifuentes IL, Silver PG (1989) Low-frequency source characteristics of the great 1960 Chilean earthquake. *J Geophys Res* 94(B1):643–663
- Dziewonski AM, Anderson DL (1981) Preliminary reference earth model. *Phys Earth Planet Inter* 25:297–356
- Gica E, Spillane MC, Titov VV, Chamberlin CD, Newman JC (2008) Development of the forecast propagation database for NOAA's short-term inundation forecast for tsunamis (SIFT), NOAA Technical Memorandum OAR PMEL-139, Pacific Marine Environmental Laboratory Seattle
- Gill AE (1982) Atmosphere-ocean dynamics. Academic Press, London
- Henry C, Das S (2001) Aftershock zones of large shallow earthquakes: fault dimensions, aftershock area expansion and scaling relations. *Geophys J Int* 147:272–293
- Ichinose G, Somerville P, Thio HK, Graves R, O'Connell D (2007) Rupture process of the 1964 Prince William Sound, Alaska, earthquake from the combined inversion of seismic, tsunami, and geodetic data. *J Geophys Res* 112:B07306. doi:10.1029/2006JB004728
- Johnson JM, Satake K (1997) Estimation of seismic moment and slip distribution of the April 1, 1946, Aleutian tsunami earthquake. *J Geophys Res* 102:11765–11774
- Johnson JM, Satake K (1999) Asperity distribution of the 1952 Great Kamchatka earthquake and its relation to future earthquake potential in Kamchatka. *Pure Appl Geophys* 154(3–4):541–553. doi:10.1007/s000240050243
- Johnson JM, Satake K, Holdahl SH, Sauber J (1996) The 1964 Prince William Sound earthquake: joint inversion of tsunami and geodetic data. *J Geophys Res* 101:523–532
- Kanamori H (1977) The energy release in great earthquakes. *J Geophys Res* 82(20):2981–2987
- Kanamori H, Cipar JJ (1974) Focal process of the great Chilean earthquake, May 22, 1960. *Phys Earth Planet Inter* 9(20):128–136
- Kirby S, Scholl D, von Heune R, Wells R, members of the USGS Tsunami Source Working Group (2013) Alaska earthquake source for the SAFRR Tsunami Scenario, chap. B. In: Ross SL, Jones LM (eds) The SAFRR (Science Application for Risk Reduction) Tsunami Scenario: U.S. Geological Survey Open-File Report 2013–1170. <http://pubs.usgs.gov/of/2013/1170/b/>
- Lay T, Kanamori H, Ammon CJ, Nettles M, Ward SN, Aster R, Beck SL, Bilek SL, Brudzinski MR, Butler R, DeShon HR, Ekström G, Satake K, Sipkin S (2005) The great Sumatra–Andaman Earthquake of 26 December 2004. *Science* 308:1127–1133
- Lay T, Ammon CJ, Kanamori H, Yamazaki Y, Cheung KF, Hutko AR (2011a) The 25 October 2010 Mentawai tsunami earthquake (Mw 7.8) and the tsunami hazard presented by shallow megathrust ruptures. *Geophys Res Lett* 38(6):L06302. doi:10.1029/2010GL046552
- Lay T, Yamazaki Y, Ammon CJ, Cheung KF, Kanamori H (2011b) The 2011 Mw 9.0 off the Pacific coast of Tohoku earthquake: comparison of deep-water tsunami signals with finite-fault rupture model predictions. *Earth, Planets Space* 63(7):797–801
- Lay T, Ammon CJ, Kanamori H, Xue L, Kim MJ (2011c) Possible large near-trench slip during the great 2011 Tohoku (Mw 9.0) earthquake. *Earth Planets Space*. doi:10.5047/eps.2011.05.033

- Lay T, Ye L, Kanamori H, Yamazaki Y, Cheung KF, Ammon CJ (2013a) The February 6, 2013 Mw 8.0 Santa Cruz Islands earthquake and tsunami. *Tectonophysics* 608:1109–1121
- Lay T, Ye L, Kanamori H, Yamazaki Y, Cheung KF, Kwong K, Koper KD (2013b) The October 28, 2012 Mw 7.8 Haida Gwaii underthrusting earthquake and tsunami: slip partitioning along the Queen Charlotte Fault transpressional plate boundary. *Earth Planet Sci Lett* 375:57–70
- López AM, Okal EA (2006) A seismological reassessment of the source of the 1946 Aleutian ‘tsunami’ earthquake. *Geophys J Int* 165:835–849. doi:10.1111/j.1365-246X.2006.02899.x
- Moreno MS, Bolte J, Klotz J, Melnick D (2009) Impact of megathrust geometry on inversion of coseismic slip from geodetic data: application to the 1960 Chile earthquake. *Geophys Res Lett* 1:L16310. doi:10.1029/2009GL039276
- Munger S, Cheung KF (2008) Resonance in Hawaii waters from the 2006 Kuril Islands Tsunami. *Geophys Res Lett* 35:L07605. doi:10.1029/2007GL032843
- National Centers for Environmental Information, National Oceanic and Atmospheric Administration. <https://www.ngdc.noaa.gov/nndc/struts/form?t=101650&s=166&d=166>. Accessed April 2016
- Okada Y (1985) Surface deformation due to shear and tensile faults in a half space. *Bull Seismol Soc Am* 75(4):1135–1154
- Okal EA, Hébert H (2007) Far-field simulation of the 1946 Aleutian tsunami. *Geophys J Int* 169:1229–1238. doi:10.1111/j.1365-246X.2007.03375.x
- Roerber V, Yamazaki Y, Cheung KF (2010) Resonance and impact of the 2009 Samoa tsunami around Tutuila, American Samoa. *Geophys Res Lett* 37(21):L21604. doi:10.1029/2010GL044419
- Tang L, Chamberlin C, Tolkova E, Spillane M, Titov VV, Bernard EN, Mofjeld HO (2006) Assessment of potential tsunami impact for Pearl Harbor, Hawaii. NOAA Technical Memorandum OAR PMEL-131, Pacific Marine Environmental Laboratory, Seattle
- Tang L, Titov VV, Chamberlin CD (2009) Development, testing, and applications of site-specific tsunami inundation models for real-time forecasting. *J Geophys Res* 114:C12025. doi:10.1029/2009JC005476
- Tanioka Y, Seno T (2001) Detailed analysis of tsunami waveforms generated by the 1946 Aleutian tsunami earthquake. *Nat Hazards Earth Syst Sci* 1:171–175
- Titov VV, González FI (1997) Implementation and testing of the method of splitting tsunami (MOST) model, NOAA technical memorandum ERL PMEL-112. NOAA Pacific Marine Environmental Laboratory, Seattle, WA, 11 pp
- Titov VV, Synolakis CS (1998) Numerical modeling of tidal wave run-up. *J Waterw Port Coast Ocean Eng* 124(4):157–171
- Titov VV, Mofjeld HO, González FI, Newman JC (1999) Offshore forecasting of Hawaiian tsunamis generated in Alaskan-Aleutian subduction zone, NOAA technical Memorandum ERL report PMEL-114, Pacific Marine Environmental Laboratory (PMEL), Seattle
- Titov VV, Mofjeld HO, González FI, Newman JC (2001) Offshore forecasting of Alaskan tsunami in Hawaii. In: Hebenstreit GT (ed) *Tsunami research at the end of a critical decade*. Kluwer Academic, Dordrecht, pp 75–90
- Titov VV, González FI, Bernard EN, Ebel JE, Mofjeld HO, Newman JC, Venturato AJ (2005) Real-time tsunami forecasting: challenges and solutions. *Nat Haz* 35:40–58
- Wei Y, Mao XZ, Cheung KF (2006) Well-balanced finite volume model for long-wave run-up. *J Waterw, Port, Coast Ocean Eng* 132(2):114–124
- Wu YY, Cheung KF (2008) Explicit solution to the exact Riemann problem and application in nonlinear shallow-water equations. *Int J Numer Methods Fluids* 57(11):1649–1668
- Yamazaki Y, Cheung KF (2011) Shelf resonance and impact of near-field tsunami generated by the 2010 Chile earthquake. *Geophys Res Lett* 38:L12605. doi:10.1029/2011GL047508
- Yamazaki Y, Kowalik Z, Cheung KF (2009) Depth-integrated, non-hydrostatic model for wave breaking and run-up. *Int J Numer Methods Fluids* 61(5):473–497
- Yamazaki Y, Cheung KF, Kowalik Z (2011a) Depth-integrated, non-hydrostatic model with grid nesting for tsunami generation, propagation, and run-up. *Int J Numer Methods Fluids* 67(12):2081–2107
- Yamazaki Y, Lay T, Cheung KF, Yue H, Kanamori H (2011b) Modeling near-field tsunami observations to improve finite-fault slip models for the 11 March 2011 Tohoku earthquake. *Geophys Res Lett* 38:L00G15. doi:10.1029/2011GL049130
- Yamazaki Y, Lay T, Cheung KF, Yue H, Kanamori H (2011c) Modeling near-field tsunami observations to improve finite-fault slip models for the 11 March 2011 Tohoku earthquake. *Geophys Res Lett* 38:L00G15. doi:10.1029/2011GL049130
- Yamazaki Y, Cheung KF, Kowalik Z, Lay T, Pawlak G (2012) NEOWAVE. In: *Proceedings and results of the 2011 NTHMP model benchmarking workshop*, Boulder: U.S. Department of Commerce/NOAA/NTHMP (NOAA Special Report), pp 239–302

- Yamazaki Y, Cheung KF, Pawlak G, Lay T (2012b) Surges along the Honolulu coast from the 2011 Tohoku tsunami. *Geophys Res Lett* 39:L09604. doi:[10.1029/2011GL050386](https://doi.org/10.1029/2011GL050386)
- Yamazaki Y, Cheung KF, Lay T (2013) Modeling of the 2011 Tohoku tsunami from finite-fault inversion of seismic waves. *Bull Seismol Soc Am* 103(28):1444–1455